Tetrahedron 69 (2013) 293–301

Contents lists available at SciVerse ScienceDirect

Tetrahedron

journal homepage: www.elsevier.com/locate/tet

Synthesis and study of novel supramolecular nanocomposites containing aryl-imidazo-phenanthroline-based metallo-polymers (H-donors) and surface-modified ZnO nanoparticles (H-acceptors)

Hsiao-Ping Fang, Yen-Hsing Wu, Hong-Cheu Lin *

Department of Materials Science and Engineering, National Chiao Tung University, Hsinchu 30049, Taiwan, ROC

ARTICLE INFO

Article history:
Received 9 August 2012
Received in revised form 20 September 2012
Accepted 9 October 2012
Available online 16 October 2012

Keywords:
Metallo-polymer
Coordination polymer
Supramolecular
Nanocomposite
H-Bonded effect
Electrochromic materials

ABSTRACT

Four novel metallo-polymers (**P1**–**P4**) containing aryl-imidazo-phenanthrolines (AIP) ligands (incorporated with phenyl and fused-thiophene cores) were synthesized and characterized. Interestingly, **P1**–**P4** exhibited electrochromism during the oxidation processes of cyclic voltammogram studies. In addition, **P1**–**P4** were blended with surface-modified pyridyl–ZnO nanoparticles (**ZnOpy** as proton acceptors) to form nanocomposites, where **P3**–**P4** were functionalized with carboxylic acid pendants (as proton donors) on the polymer backbones to study for the H-bonded effects on surface-modified **ZnOpy** nanoparticles. In order to investigate the nanocomposites containing metallo-polymers **P1**–**P4** and surface-modified **ZnOpy** nanoparticles, nanocomposites **P1**–**P4**/**ZnOpy** were characterized by UV–visible (UV) absorption spectra, Fourier transform infrared (FT-IR), photoluminescence (PL) spectra, time-resolved photoluminescence decays, X-ray diffraction (XRD) measurements, and transmission electron microscopy (TEM) analyses. In contrast to nanocomposites **P1**/**ZnOpy** and **P2**/**ZnOpy**, higher crystallinities with a distinct layered-structure of H-bonded nanocomposites **P3**/**ZnOpy** and **P4**/**ZnOpy** in XRD measurements were induced by the introduction of surface-modified **ZnOpy** nanoparticles to metallo-polymers **P3** and **P4**, correspondingly. Furthermore, due to the supramolecular interactions of surface-modified **ZnOpy** nanoparticles with metallo-polymers **P3**–**P4**, TEM images verified that **ZnOpy** nanoparticles were more homogeneously distributed in nanocomposites **P3**–**P4**/**ZnOpy** (with H-bonds) than those in **P1**–**P2**/**ZnOpy** (without H-bonds), respectively.

© 2012 Elsevier Ltd. All rights reserved.

1. Introduction

Metal–ligand coordination seems to be particularly attractive in past few decades because of searching for new smart materials.[1–3] In recent years, the researches on supramolecular metallo-polymers applied to electro-optical materials have been commonly conducted, because the advantages of these materials, such as easy processability, cheap fabrication, rapid coordination, and tunability of the optical band gap, can promote long-range electrons or energy transfers.[4] Supramolecular metallo-architecture is formed with coordination ability of transition metal ions and chelating ligands because of their self-recognition and self-assembly.[5–7] Moreover, metal–ligand complexes realized ideal conditions from self-assembly to form the kinetically labile but nevertheless thermodynamically stable bonds.[8] In the meanwhile, metallo-polymers are also good candidates to study for their electrochromic properties during the redox processes.[9]

2,2′:6′,2″-Terpyridine(terpy), diaminopyridine (dap), bis(porphyrin)pyrazines, and bipyrdine (bpy) derivatives have been utilized recently for multinuclear supramolecular interactions.[10–13] In this context, bipyrdine derivatives (i.e., 1*H*-imidazo[4,5-*f*][1,10]phenanthrolines)[14] with metal–ligand coordination seem to open an alternative path to produce conjugated polymers, and aryl-imidazo-phenanthroline ligands are ideally suitable for the construction of coordination polymers. Additionally, the easy synthetic access of aryl-imidazo-phenanthroline ligands offers the construction of perfect rods or dendrimers in coordination polymers. 1*H*-Imidazo[4,5-*f*][1,10]phenanthroline is one of the metal–ligand combination units that have been of particular importance for the construction of metallo-supramolecular polymers. During the process of light emission in the fully conjugated metallo-polymers, it was confirmed that the phenomenon of metal to ligand charge transfer (MLCT) occurred in 1*H*-imidazo[4,5-*f*][1,10]phenanthroline–Ru(II) moieties. A series of aryl-imidazo-phenanthrolines–Ru(II) metallo-polymers, including benzene[14b] and fused dithiophene[15] units as building blocks, were constructed by self-assembled reactions. Two conjugated spacers, i.e., benzene and fused dithiophene segments, were inserted between two

* Corresponding author. Tel.: +886 3 5712121x55305; fax: +886 3 5724727; e-mail address: linhc@mail.nctu.edu.tw (H.-C. Lin).

0040-4020/$ – see front matter © 2012 Elsevier Ltd. All rights reserved.
http://dx.doi.org/10.1016/j.tet.2012.10.031

imidazo-phenanthroline chelating units to form the main structures of ligands **L1** and **L2**, respectively. Hence, the lengths of conjugations in **L1** and **L2** linked by conjugated spacers were extended in order to improve the electric charge transfer abilities and to enhance the absorption intensities and ranges. The transport of energy and electrons within nanoscale ordered materials are significant to optoelectronics. It needs to control over both of their physical and chemical properties in the self-assembled organization. Nanocomposite systems are that combine the favorable features of, for example, fullerenes and porphyrins as electron acceptors and donors, respectively.[10] They have received interest in the areas of light-induced electron-transfer chemistry and solar energy conversion.[16] Common electron donor–acceptor systems are based on covalent linkages. However, much less is, known about noncovalent electron donor–acceptor nanocomposites and the function of the intervening spacers.[17] Compared with other intermolecular forces, such as van der Waals, π–π stacking, or Coulombic interactions, hydrogen bonds are particularly attractive as they are directional and do not possess electronic energy levels that interfere with those in materials for organic electro-optical applications.[18,19] Therefore, that great efforts have been expended toward the preparation and characterization of photo- and electroactive noncovalent assemblies based on hydrogen bonds (H-bonds).

Herein, we design H-bonded interactions between pyridyl surface-modified **ZnOpy** nanoparticles (**ZnOpy** as proton acceptors) and metallo-polymers (**P3**–**P4** as proton donors) (Fig. 1). Because supramolecular interactions (H-bonds) between **ZnOpy** and metallo-polymers turn the organic and inorganic interfaces into homogeneous dispersion, electron and hole separations are improved to enhance electric translation and reduce electric recombination. The environmentally friendly and low-cost ZnO nanoparticles offer a new perspective candidate toward 'green electricity'. By mixing **ZnOpy** nanoparticles as proton acceptors, i.e., a substance with a higher affinity with the polymer, it is possible to break up the excitons by transferring the electrons from the polymers onto the electron acceptors.[20]

2. Results and discussion

2.1. Syntheses and chemical characterization

Metallo-polymers **P1**–**P4** were prepared successfully via coordination with a mixture of ligands 2-(4-(1*H*-imidazo[4,5-*f*][1,10]phenanthrolin-2-yl)-2,5-bis(octyloxy)phenyl)-1*H*-imidazo[4,5-*f*][1,10]phenanthroline (**L1**) and 2-(4-(1*H*-imidazo[4,5-*f*][1,10]phenanthrolin-2-yl))-3,5 (dihexyldithieno[3,2-*b*:2′3′-*d*]thioeno)-1*H*-imidazo[4,5-*f*][1,10]phenanthroline (**L2**). The integration of ^{1}H NMR spectra reveal a facile result to distinguish the well-defined main-chain metallo-polymeric structures, which were constructed by different ligands. Proton NMR spectra of ligands **L1**–**L2** and metallo-polymers **P1**–**P4** in DMSO are illustrated in Figs. 2 and 3, which show proton peaks in the aromatic regions of ligands and metallo-polymers. As a result of metallo-polymerization, broadened signals of ligands were observed. Ligands **L1**–**L2** and metallo-polymers **P1**–**P4** were satisfactorily characterized by ^{1}H NMR spectra. The thermal stabilities of metallo-polymers **P1**–**P4** were characterized by thermogravimetric analyses (TGA) measurements under nitrogen atmosphere, and the thermal decomposition temperatures (T_d) are in the range of 320–380 °C.

2.2. UV spectroscopic studies

The absorption spectral data of all metallo-polymers **P1**–**P4** and ligands **L1**–**L2** in DMF solutions (10^{-6} M) and solid films are

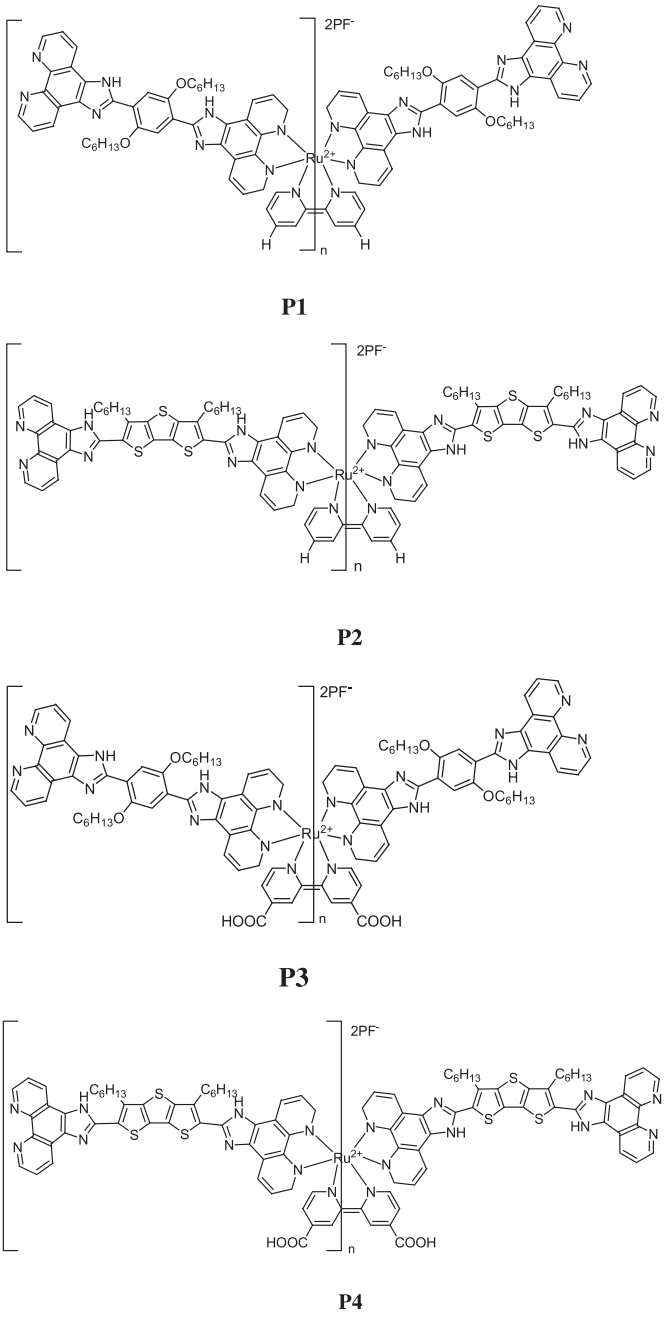

Fig. 1. Chemical structures of metallo-polymers **P1**–**P4**.

summarized in Fig. 4 and Table 1. The absorption wavelengths of metallo-polymers (**P1**–**P4**) in Fig. 4 exhibit broad wavelength ranges from 270 to 650 nm. Similar to the absorption peaks of ligands (**L1**–**L2**) ca. 280 and 380 nm in Fig. 4, all short absorption peaks of metallo-polymers (**P1**–**P4**) in the range of 270–490 nm were due to the dπ→π* transitions. These intramolecular charge transfer (ICT) results show that the maximum absorption wavelengths of **P2** (429 nm) and **P4** (407 nm) are longer than those of polymers **P1** (385 nm) and **P3** (343 nm), respectively, which reflects the longer effective conjugation lengths existing in the extended fused-thiophene-based polymers (**P2** and **P4**). Moreover, the characteristic absorption bands of metallo-polymers (**P1**–**P4**) in the range of 490–560 nm are attributed to the metal-to-ligand charge transfer (MLCT) transition. According to Fig. 4(b), the optical band gaps (in Table 1) can be estimated from the absorption spectra in solid films by using the equation of E_g=1240/λ_{edge}. As

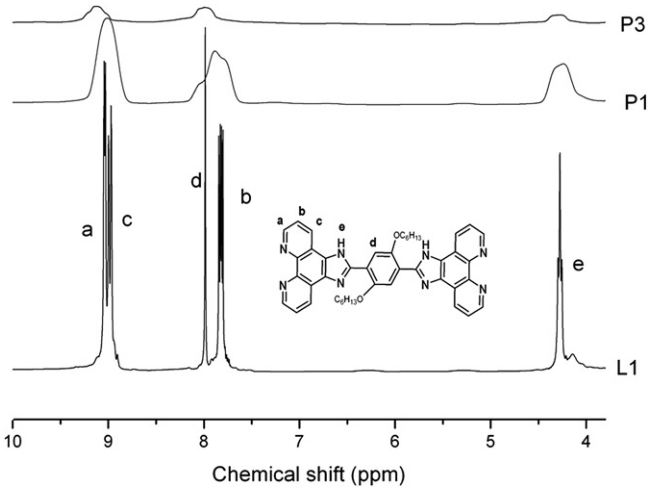

Fig. 2. ^{1}H NMR spectra (aromatic region) of ligand **L1** and metallo-polymers **P1** and **P3** in DMSO-d_6.

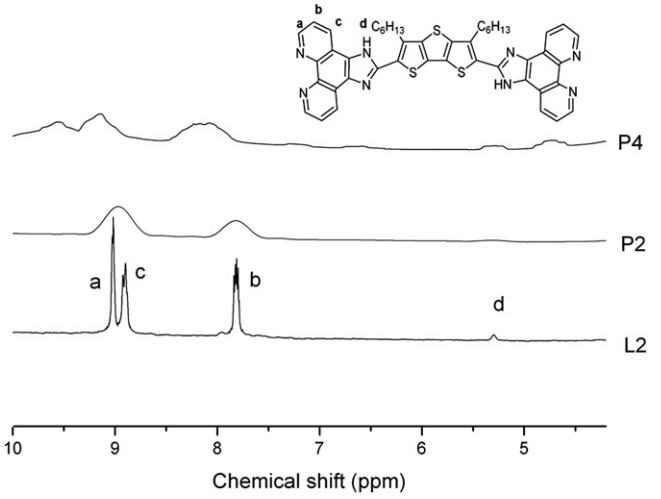

Fig. 3. ^{1}H NMR spectra (aromatic region) of ligand **L2** and metallo-polymers **P2** and **P4** in DMSO-d_6.

shown in Table 1, the band gaps of metallo-polymers (**P1**–**P4**) are compared to have the sequence of **P4**<**P3**=**P2**<**P1** and with the largest value in **P1** and the smallest value in **P4**. Therefore, the band gaps of metallo-polymers can be reduced by the replacement of phenyl rings (**P1** and **P3**) with thiophene rings (**P2** and **P4**), and the replacement of the H atoms (**P1** and **P2**) with the COOH groups (**P3** and **P4**).

2.3. Electrochemical characterization

The electronic states, i.e., energy levels of the highest occupied molecular orbital (HOMO) and lowest unoccupied molecular orbital (LUMO), of the metallo-polymers were investigated by cyclic voltammetry (CV) in order to understand the charge injection processes in these metallo-polymers. The electrochemical responses of Ru(II) polypyridyl complexes were usually observed due to a metal-centered oxidation, and thus to induce the electrochromic behavior.[21] The oxidation cyclic voltammograms and corresponding electrochromic photos of metallo-polymers **P1**–**P4** in solid films are displayed in Fig. 5(a). The formal potentials, onset potentials, and band gaps, along with the estimated positions of the upper edges of the valence band (HOMO) obtained from the electrochemical measurements are summarized in Table 1. The ligands

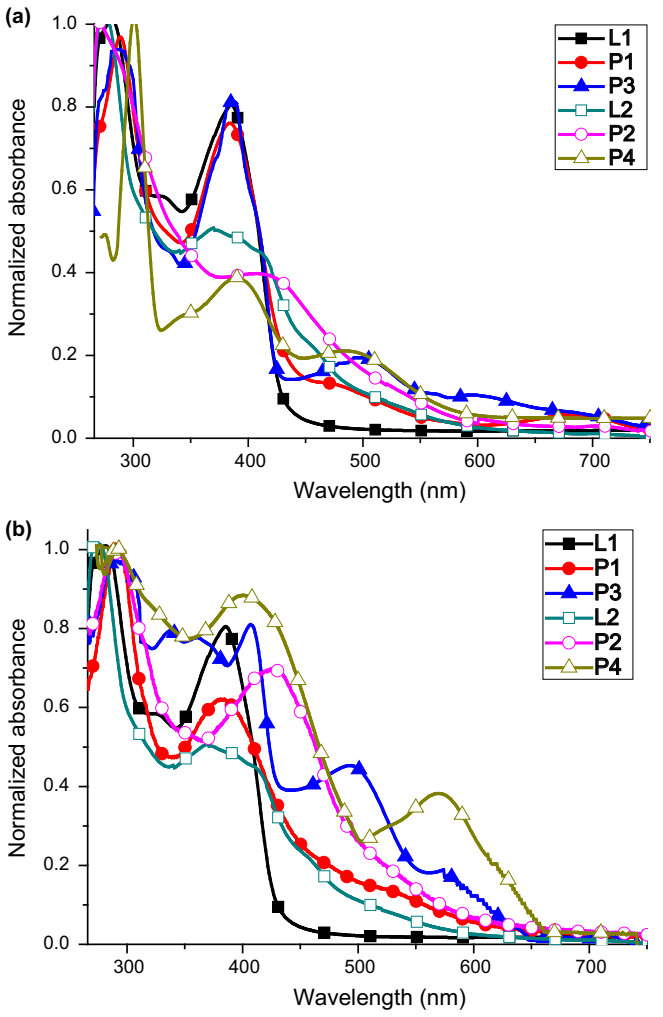

Fig. 4. Normalized UV–vis spectra of ligands **L1**–**L2** and metallo-polymers **P1**–**P4** in (a) DMF solutions and (b) solid films.

Table 1
Photophysical data in DMF solutions and solid films and electrochemical potentials, energy levels, and band gap energies of metallo-polymers **P1**–**P4**[a]

Samples	λ, UV (nm)		Energy level[b]	Energy level	Band gap
	Solution	Solid film[a]	E_{HOMO} (eV)[c]	E_{LUMO} (eV)[e]	$E_{g,opt}$ (eV)[d]
L1	285, 384,	281, 385	—	—	2.8
L2	281, 377	275, 378	—	—	2.1
P1	288, 387, 490	292, 385, 517	5.1	2.6	2.5
P2	276, 420, 516	289, 429, 517	5.93	3.93	2.0
P3	286, 385, 506	293, 343, 503	5.91	3.91	2.0
P4	298, 390, 490	286, 407, 572	5.7	3.8	1.9

[a] Spin-coated from DMF solution.
[b] Measured for in thin solid film using tetra-*n*-butylammonium perchlorate (TCI) as the supporting electrolyte at a scan rate of 100 mV/s.
[c] HOMO=[−($E_{onset\ (vs\ Ag/AgCl)}$−$E_{onset\ (Fc/Fc+vs\ Ag/AgCl)}$)−4.8] eV where 4.8 eV is the energy level of ferrocene below the vacuum level and $E_{onset\ (Fc/Fc+vs\ Ag/AgCl)}$=0.4 eV.
[d] Optical band gaps were estimated from the absorption spectra in solid films by using the equation of E_g=1240/λ_{edge}.
[e] E_{LUMO}=E_{HOMO}+$E_{g,opt}$.

(**L1**, **L2**) showed no detectable oxidation and reduction behavior, implying that the electrons are difficult to be injected into both ligands (**L1**, **L2**). As shown in Fig. 5(a), metallo-polymers **P1**–**P4** showed one irreversible oxidation process but no detectable reduction behavior. Therefore, the HOMO energy levels of **P1**–**P4** can

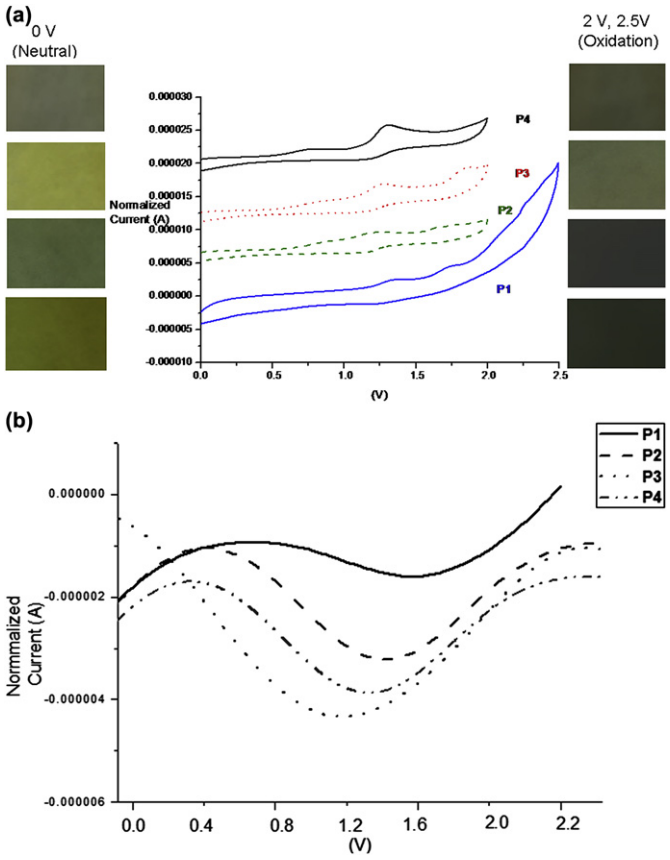

Fig. 5. (a) Cyclic voltammagrams and electrochromic photos and (b) differential pulse voltammetric (DPV) of metallo-polymers **P1**–**P4** in solid films.

be decided by their irreversible oxidation peaks correspondingly. In addition, as shown in Fig. 5(b), differential pulse voltammetric (DPV) studies on metallo-polymers **P1**–**P4** were performed under analogous conditions of CV measurements, and DPV results also confirmed the results of CV measurements as illustrated in Fig. 5(a).

2.4. FT-IR spectroscopic studies

The molecular structures of metallo-polymers **P1**–**P4** could also be confirmed by the FT-IR spectra. For instance, the absorption stretching mode of the carboxylic group in the polymers, which typically appeared at 1710, 1642 cm^{-1}, respectively, was absent in the spectra of metallo-polymers **P3**–**P4**. Supramolecular structures of H-bonded nanocomposites are displayed in Fig. 6. H-bonded effects in H-donor metallo-polymers (**P3**–**P4**) blended with H-acceptor **ZnOpy** nanoparticles were confirmed by FT-IR spectroscopy. The IR spectra of H-acceptor **ZnOpy**, H-donor metallo-polymers **P3**–**P4**, and their H-bonded nanocomposites **P3**–**P4**/**ZnOpy**, shown in Fig. 7, were compared to analyze the formation of H-bonds. In contrast to the O–H bands at 2665 and 2620 cm^{-1} of pure H-donor polymers **P3** and **P4**, weaker O–H bands were observed at 2513, 2500 cm^{-1} and 1921, 1935 cm^{-1} in H-bonded nanocomposites **P3**/**ZnOpy** and **P4**/**ZnOpy**, respectively. These results are indicative of stronger H-bonds formed between pyridyl groups of H-acceptor **ZnOpy** and acid groups of H-donor metallo-polymers **P3**–**P4** in their H-bonded nanocomposites **P3**–**P4**/**ZnOpy**. On the other hand, C=O stretching vibrations at 1710 and 1642 cm^{-1} in pure metallo-polymers **P3** and **P4** appeared as shoulders at 1736 and 1635 cm^{-1} for H-bonded nanocomposites **P3**–**P4**/**ZnOpy**, respectively. This shows that the carbonyl group is in a more associated state than that in the pure H-donor metallo-polymers

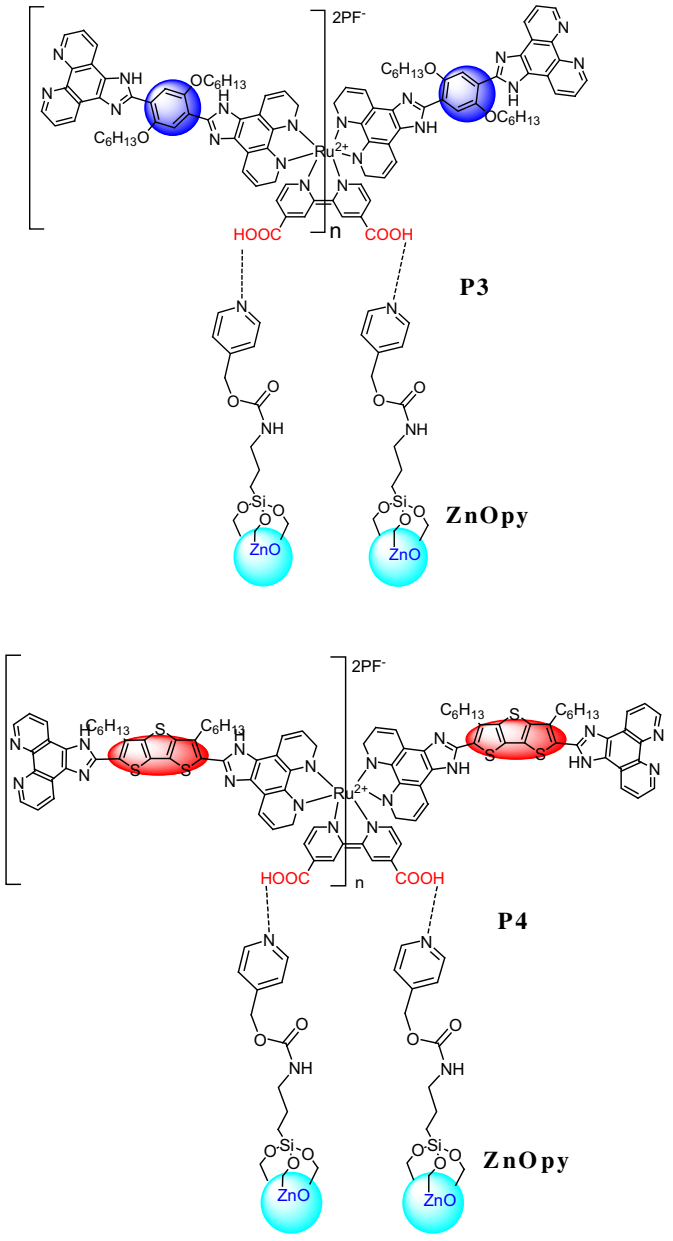

Fig. 6. Supramolecular structures of H-bonded nanocomposites **P3**/**ZnOpy** and **P4**/**ZnOpy**.

P3–**P4**, which contains a weaker C=O stretching vibration appeared (at 1710 and 1642 cm^{-1}). All results suggest that H-bonds were generated in the solid state of H-bonded nanocomposites **P3**/**ZnOpy** and **P4**/**ZnOpy**, which is similar to our previous report.[22]

2.5. Time-resolved PL spectroscopic studies

The photoluminescence (PL) spectra of metallo-polymers **P1**–**P4** (Fig. 8(a)) and H-bonded nanocomposites **P1**–**P4**/**ZnOpy** (Fig. 8(b)) in solid films were excited at an incident wavelength of 420 nm. Their PL emissions show broad and weak absorptions from 420 to 650 nm, which covered all PL ranges of metallo-polymers **P1**–**P4** and nanoparticle **ZnOpy**. Time-resolved photoluminescence (PL) measurements (i.e., ultrafast emission dynamics), monitored at the wavelength above 420 nm, were (Fig. 9(b)) were 3.8, 5.0, 1.6, and 2.3 ns, respectively, and those of metallo-polymers **P1**–**P4** were 7.1, 6.9, 7.0, and 7.0 ns, respectively

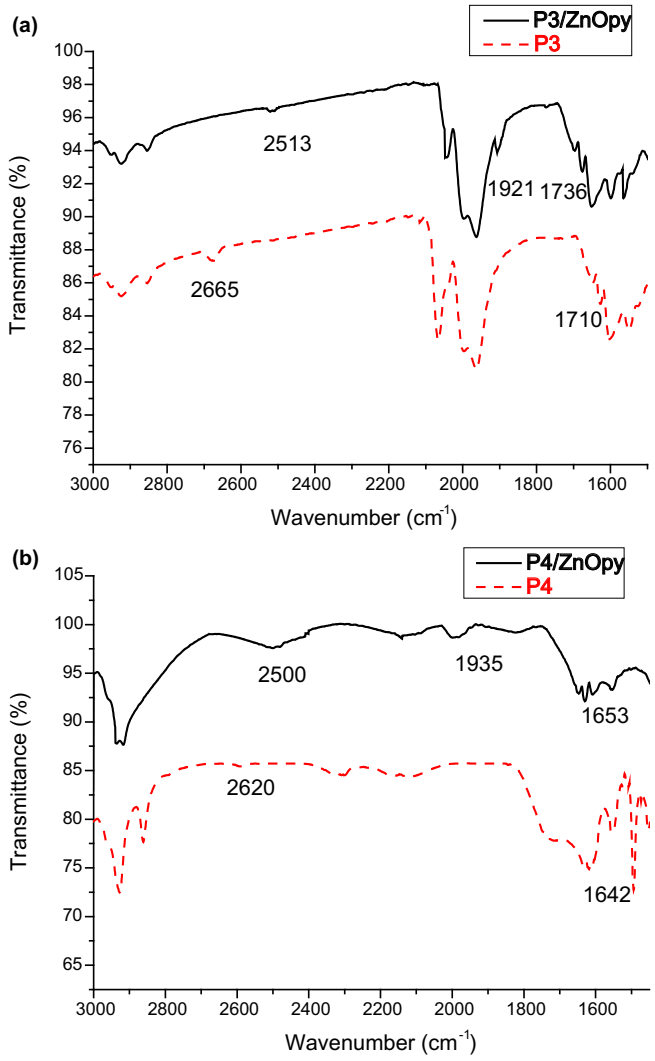

Fig. 7. FT-IR spectra of metallo-polymers (**P3** and **P4**) and nanocomposites (**P3**/**ZnOpy** and **P4**/**ZnOpy**).

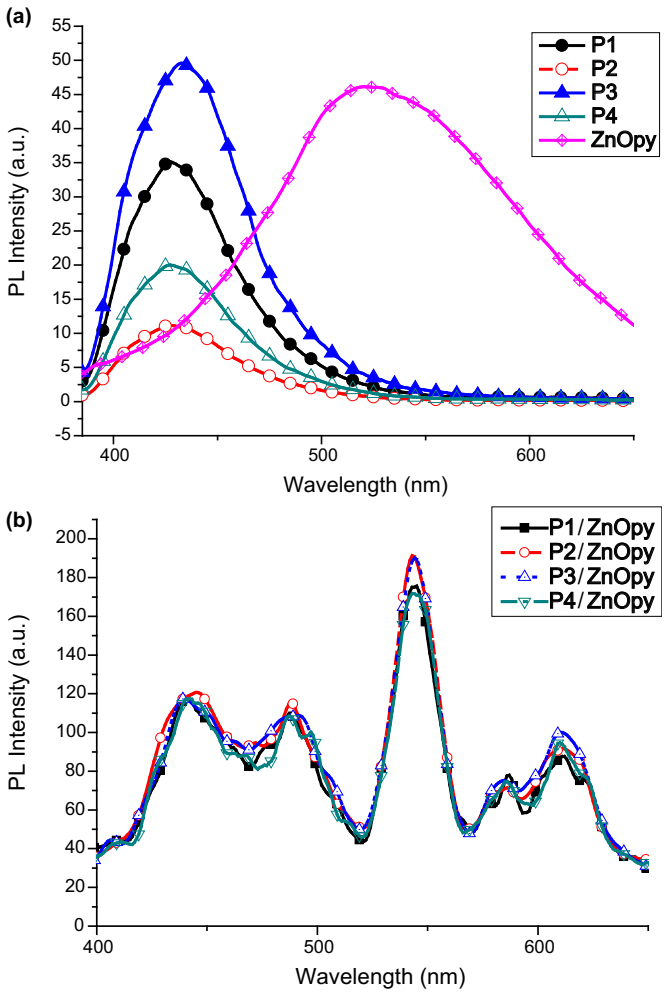

Fig. 8. PL spectra of metallo-polymers (a) **P1**–**P4** and nanocomposites (b) **P1**/**ZnOpy**, **P2**/**ZnOpy**, **P3**/**ZnOpy**, and **P4**/**ZnOpy**.

(Fig. 9(a)). The faster PL decay of nanocomposites **P1**–**P4**/**ZnOpy** than those of metallo-polymers **P1**–**P4** can be attributed to the quenching behavior from nanoparticle **ZnOpy**. More importantly, improving interfacial contacts by H-bonds between polymers and nanoparticle **ZnOpy**, H-bonded nanocomposites **P3**/**ZnOpy** and **P4**/**ZnOpy** have shorter lifetime values (1.6, and 2.3 ns) than nanocomposites **P1**/**ZnOpy** and **P2**/**ZnOpy** (3.8, and 5.0 ns), respectively. These results suggest that the excitons are easier to be quenched via the H-bonded interfaces of polymers and nanoparticles, which were also reported as a more rapid charge transfer process from P3HT to CdSe with a surface modification [24]performed to give additional information on the charge-transfer dynamics in nanocomposites **P1**–**P4**/**ZnOpy** by measuring the fluorescence lifetimes using time-correlated single-photon counting (TCSPC) methodology (Fig. 9). The apparatus for the TCSPC measurements was described in the literature.[23] As illustrated in Table 2, the measurements revealed that the luminescence lifetime values of nanocomposites **P1**–**P4**/**ZnOpy**.

2.6. X-ray diffraction (XRD) analyses

In order to investigate the microstructural orders and molecular arrangements of nanocomposites **P1**–**P4**/**ZnOpy** (with or without H-bonded interactions) in solids, X-ray diffraction (XRD) measurements were also performed on powder samples of metallo-polymers **P1**–**P4** and nanoparticle **ZnOpy**, and all powder XRD spectra are illustrated in Fig. 10. The annealed **P3**/**ZnOpy** (Fig. 10(c)) and **P4**/**ZnOpy** (Fig. 10(d)) films exhibited substantially a primary diffraction feature at 2θ=5.0° (corresponding to a smaller *d*-spacing value of 12.0 Å).[25] Compared with the amorphous halos of metallo-polymers **P3**–**P4**, the much stronger (100) reflection characteristic peaks of metallo-polymers **P3**–**P4** in nanocomposites **P3**–**P4**/**ZnOpy** (with H-bonds) were observed.

However, only weaker or no (100) reflection characteristic peaks of metallo-polymers **P1**–**P2** in nanocomposites **P1**–**P2**/**ZnOpy** (without H-bonds) were detected. The characteristic peaks were assigned to a distance between the conjugated backbones separated by the long side chains as reported for other similar π-conjugated polymers with long pendants.[26,27] The XRD data demonstrate the existence of the H-bonded interactions between metallo-polymers **P3**–**P4** and nanoparticle **ZnOpy**. In other words, the crystallinities of metallo-polymers **P3**–**P4** were enhanced upon addition of nanoparticle **ZnOpy**. The similar result was also reported that the crystallinity of P3HT polymer was increased upon addition of BT4T (a small organic molecule), which, in turn, enhanced the photovoltaic properties of the solar cell device.[28] For metallo-polymers **P1**–**P4**, the broad peaks in the wide angle region of the diffraction features at 2θ=13.7°, corresponding to the *d*-spacing values between 4.1 and 4.4 Å, and it is reasonable to assign

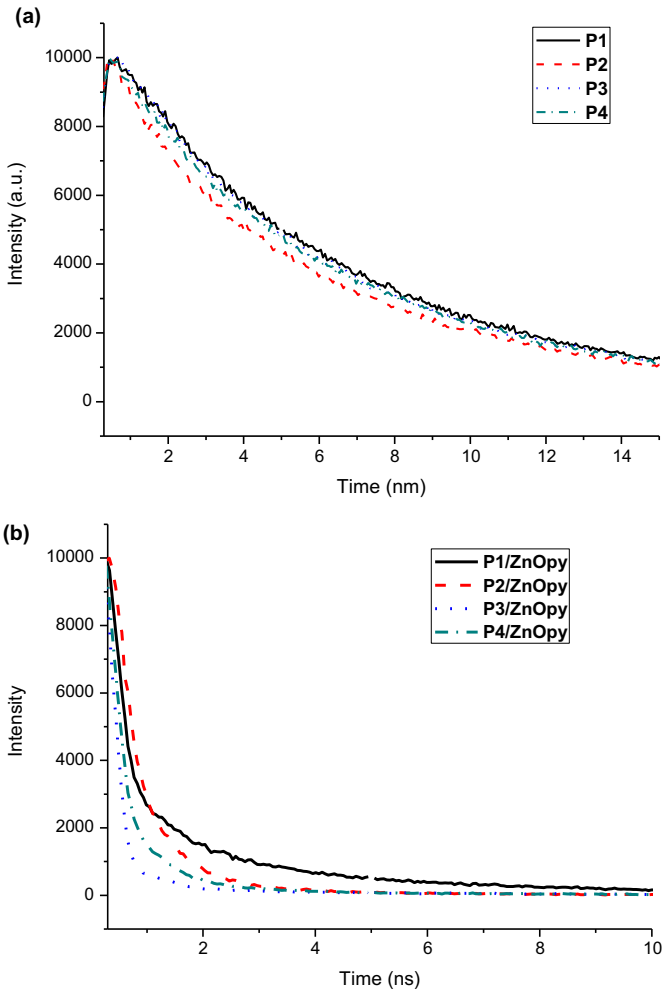

Fig. 9. Normalized time-resolved photoluminescence decays of (a) metallo-polymers **P1**–**P4** and (b) nanocomposites **P1**/**ZnOpy**, **P2**/**ZnOpy**, **P3**/**ZnOpy**, and **P4**/**ZnOpy**.

Table 2
Fluorescence lifetimes of metallo-polymers **P1**–**P4** and its nanocomposites

Sample	P1	P2	P3	P4	P1/ZnOpy	P2/ZnOpy	P3/ZnOpy	P4/ZnOpy
τ (ns)	7.1	6.9	7.0	7.0	3.8	5.0	1.6	2.3

them to the distance between disordered alkyl chains, although the peaks may also contain contributions from the layer-to-layer π–π stacking of the polymer planes.[29] The broad XRD halos indicated that the layer-to-layer π–π stacking in the polymers occurs only in very small areas, and the polymers mainly show amorphous structure.[30–32] The possible packing motifs (side-view) and the proposed model can explain the possible structural arrangements of the polymer chains in nanocomposites **P3**–**P4**/**ZnOpy**, where the alkyl side chains stack as bi-layered packings and may have trivial interdigitated arrangements, and their schematic packings are demonstrated in Fig. 11. Overall, based on the observation, it reveals that metallo-polymers **P3**–**P4** form higher crystallinity upon addition of **ZnOpy** in nanocomposites **P3**–**P4**/**ZnOpy** (with H-bonds) in contrast to amorphous **P3**–**P4**.

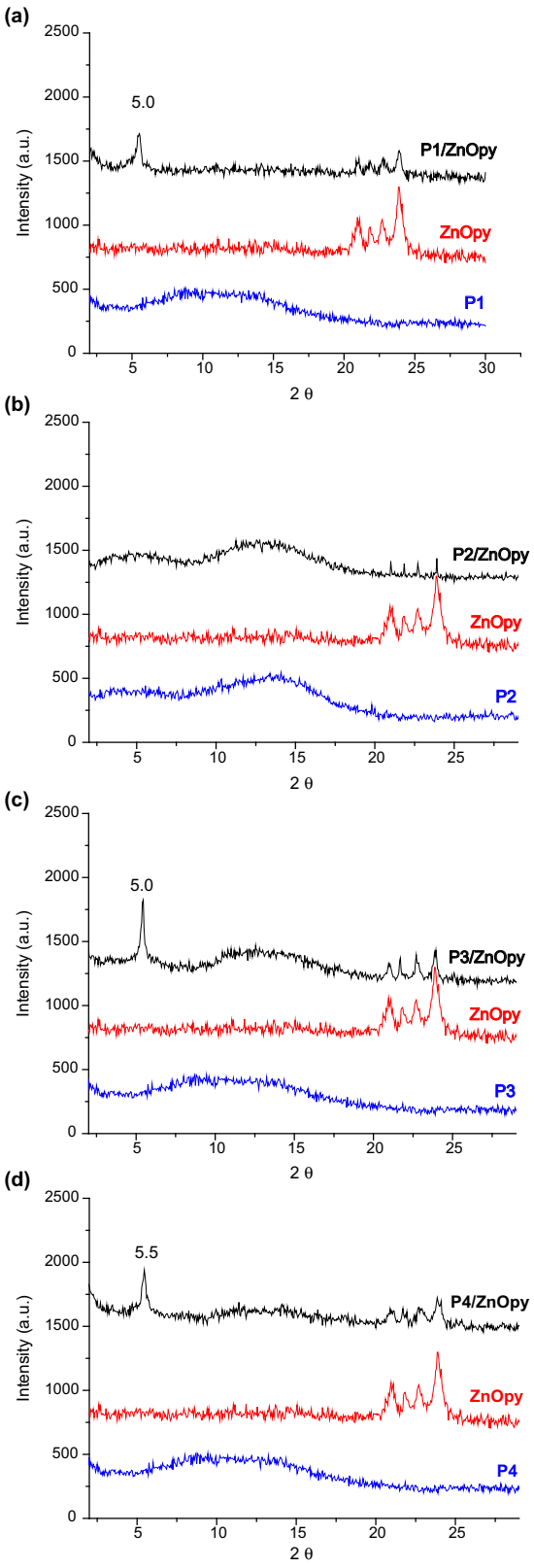

Fig. 10. Powder X-ray diffraction spectra of nanocomposites (a) **P1**/**ZnOpy**, (b) **P2**/**ZnOpy**, (c) **P3**/**ZnOpy**, and (d) **P4**/**ZnOpy**.

2.7. Transmission electron microscopy studies

Transmission electron microscopy (TEM) analyses were carried out on nanocomposites **P1**–**P4**/**ZnOpy** (with or without H-bonded interactions) in solids, which were prepared from DMF solutions of **P1**–**P4**/**ZnOpy** drop-cast onto TEM grids. This provides a further insight into the morphology of the nanoparticle aggregation. Compared with nanocomposite **P3**/**ZnOpy** (with H-bonds) in Fig. 12(c),

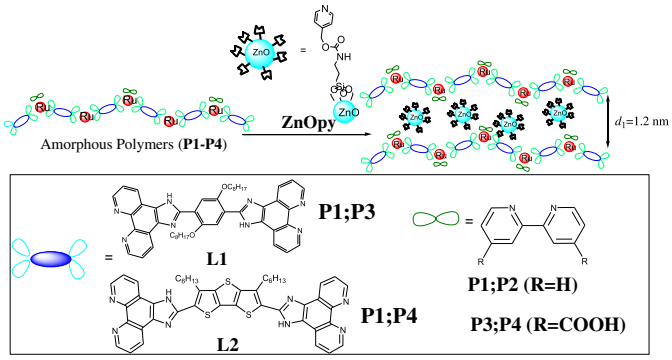

Fig. 11. Schematic illustrations of possible structural arrangements for polymer chains in nanocomposites by powder X-ray diffractions.

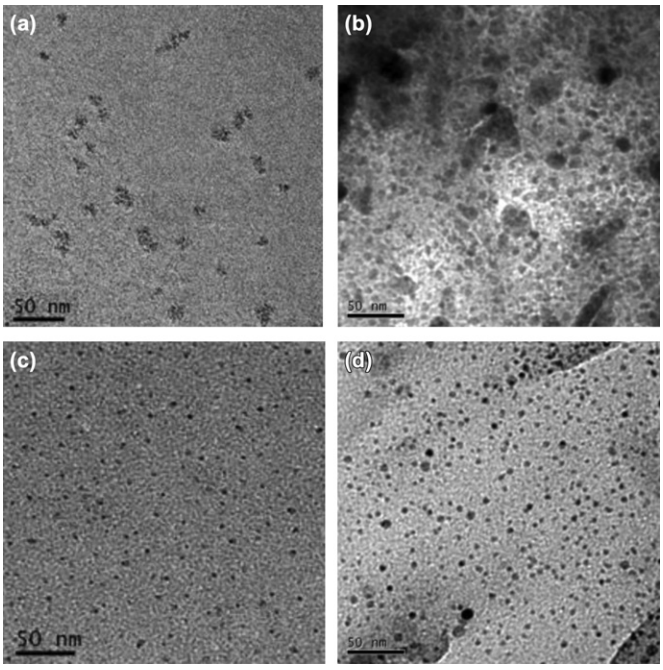

Fig. 12. TEM images of nanocomposites (a) **P1**/**ZnOpy**, (b) **P2**/**ZnOpy**, (c) **P3**/**ZnOpy**, and (d) **P4**/**ZnOpy**.

nanocomposite **P1**/**ZnOpy** (without H-bonds) had a more distinct aggregated structure in Fig. 12(a). This was due to the pyridyl H-acceptors of **ZnO** self-assembled with H-donors of metallo-polymer **P3**. This result is similar to a previous report in CdSe-L2,[33] where a conjugated polymer was functionalized via the introduction of appropriate anchoring groups to avoid the phase separation.[34] On the other hand, as **ZnOpy** nanoparticles were blended with metallo-polymer **P4**, the carboxylic acid surfactants from metallo-polymer **P4** were H-bonded with the pyridyl H-acceptor groups of **ZnOpy**. Therefore, in contrast to **P2**/**ZnOpy** (without H-bonds) in Fig. 12(b) **ZnOpy** nanoparticles were well distributed among metallo-polymer **P4** in Fig. 12(d). Hence, the TEM morphologies of H-bonded architectures in nanocomposites **P3**–**P4**/**ZnOpy** (with H-bonds) demonstrate the versatility of the self-assembled processes by the supramolecular interactions of H-donor metallo-polymers **P3**–**P4** and H-acceptor nanoparticle **ZnOpy**.

3. Conclusion

We synthesized a series of metallo-polymers (**P1**–**P4**) with arylimidazo-phenanthrolines (AIP) units (incorporated with phenyl and fused dithienothiophene groups in different donor spacers) to study for their electrochemical and electrochromic properties. In order to investigate the energy transfers between metallo-polymers (**P1**–**P4**) and nanoparticle **ZnOpy**, novel supramolecular nanocomposites **P3**–**P4**/**ZnOpy** were constructed by complexation of proton donor (H-donor) metallo-polymers **P3**–**P4**, consisting of carboxylic acid groups, with proton accepter (H-accepter) **ZnOpy**. They were compared with nanocomposites **P1**–**P2**/**ZnOpy** containing metallo-polymers **P1**–**P2** without carboxylic acid groups to have no H-bonded interactions with nanoparticle **ZnOpy**. In contrast to amorphous metallo-polymers **P3**–**P4** from XRD measurements, supramolecular nanocomposites **P3**–**P4**/**ZnOpy** exhibited obvious diffraction features (originated from metallo-polymers **P3**–**P4**) indicating the increased crystallinities of **P3**–**P4** upon addition of **ZnOpy**, due to the supramolecular (H-bonded) interactions. TEM morphologies also proved that the supramolecular (H-bonded) interactions between **ZnOpy** and polymers **P3**–**P4** induce nanoparticles to be homogeneously dispersed in nanocomposites **P3**–**P4**/**ZnOpy**.

4. Experimental section

4.1. Materials

All chemicals and solvents were used as received. The rubipyridine (Rupby), 1,10-phenanthroline-5,6-dione,[14b] 2,5-bis(octyloxy) benzene-1,4-dialdehyde,[16a] and 3,5-dihexyldithieno[3,2-*b*:2′3′-*d*] thiophene-2,6-dialdehyde[15a] were prepared according the reported literature procedure. The synthetic routes of ligands **L1**–**L2** and metallo-polymers **P1**–**P4** are shown in Scheme 1, and the synthetic procedures of their intermediates are described. Solvents were reagent grades and purchased from Aldrich, ACROS, TCI, and Lancaster Chemical Co. Toluene, *N*,*N*-dimethylformamide, and diethyl ether were distilled to keep anhydrous before use. Furthermore, **ZnO** nanoparticles were synthesized and surface-modified with pyridyl surfactants (**ZnOpy**) to be ca. 3–4 nm.[20]

4.2. Characterization

^{1}H NMR spectra were recorded on a Varian Unity 300 MHz spectrometer using DMSO-d_6 solvents. Transition temperatures were determined by differential scanning calorimetry (DSC, Perkin–Elmer Pyris 7) with a heating and cooling rate of 10 °C/min. Thermogravimetric analyses (TGA) were conducted with a TA instrument Q500 at a heating rate of 10 °C/min under nitrogen. UV–visible absorption and photoluminescence (PL) spectra were recorded in dilute *N*,*N*-dimethylformamide (DMF) solutions (10^{-5} M) on a HP G1103A and Hitachi F-4500 spectrophotometer, respectively. Solid films of UV–vis and PL measurements were spin-coated on a quartz substrate from DMF solutions with a concentration of 10 mg/mL. Cyclic voltammetry (CV) measurements were performed using a scanning rate of 100 mV/s on a BAS 100 electrochemical analyzer, which was equipped with a standard three-electrode electrochemical cell in a 0.1 M tetra-*n*-butylammonium perchlorate (TCI) solution (in DMF) at room temperature. A platinum wire as the counter electrode, and a silver wire as the quasi-reference electrode were used. Ag/AgCl (3 M KCl) electrode was served as a reference electrode for all potentials quoted herein. During the CV measurements, the solutions were purged with nitrogen for 30 s, and the redox couple ferrocene/ferrocenium ion (Fc/Fc^+) was used as an external standard. The corresponding HOMO levels in polymer solutions of **P1**–**P4** could be calculated from $E_{ox/onset}$ values of the electrochemical experiments (but no reduction curves, i.e., no $E_{red/onset}$ values and LUMO levels, were obtained in the CV measurements). Each onset potential in the CV measurements was

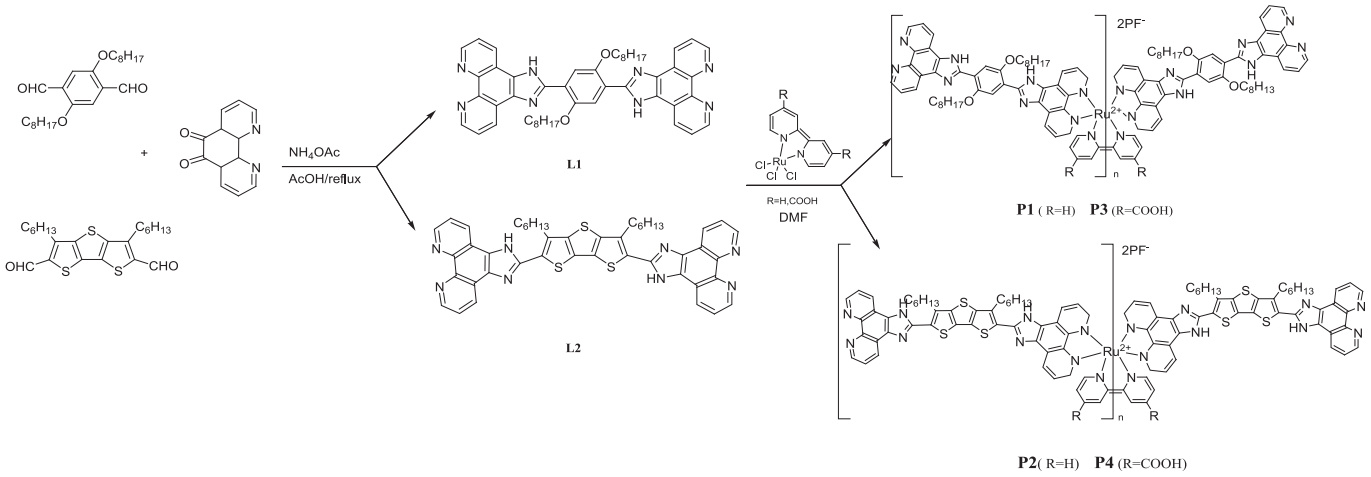

Scheme 1. Synthesis of ligands **L1**–**L2** and metallo-polymers **P1**–**P4**.

defined by the intersection of two tangents drawn at the rising current and background current. Differential pulse voltammograms (DPV) experiments were performed with a CH Instruments electrochemical analyzer. All measurements were carried out at room temperature with a conventional three electrode configuration consisting of a platinum working electrode, a platinum wire auxiliary electrode, and a nonaqueous $Ag/AgNO_3$ reference electrode. The solvent used in all experiments was DMF, and the supporting electrolyte was 0.1 M tetrabutylammonium hexafluorophosphate. Infrared spectra (FT-IR) were investigated by a Perkin–Elmer Spectrum 100 instrument. Synchrotron powder X-ray diffraction (XRD) measurements were performed at beamline BL13A of the National Synchrotron Radiation Research Center (NSRRC), Taiwan, where the wavelength of X-ray was 1.026503 Å. TEM studies were performed using a JEOL 2010 instrument under an acceleration voltage of 200 kV. The samples were prepared by dispersing into DMF and then dropping the dispersion onto the TEM copper grids. UV–visible absorption and photoluminescence (PL) spectra were recorded in dilute DMF solutions (10^{-6} M) on a HP G1103A and Hitachi F-4500 spectrophotometer, respectively. Time-resolved photoluminescence (TRPL) spectra were measured using a home-built single photon counting system. Excitation was performed using a 375 nm diode laser (Picoquant PDL-200, 50 ps fwhm, 2 MHz). The signals collected at the excitonic emissions of solutions (λ=420 nm) were connected to a time-correlated single photon counting card (TCSPC, Picoquant Timeharp 200).

4.3. Ligand synthesis

*4.3.1. 2-(4-(1H-Imidazo[4,5-f][1,10]phenanthrolin-2-yl)-2,5-bis(octyloxy)phenyl)-1H-imidazo[4,5-f][1,10]phenanthroline (**L1**).* A mixture of 1,10-phenanthroline-5,6-dione (211.2 mg, 1.0 mmol), 2,5-bis(octyloxy)benzene-1,4-dialdehyde[16a] (218.1 mg, 1.0 mmol), ammonium acetate (1557.3 mg, 20.2 mmol) and glacial acetic acid (30 ml) was refluxed for 2 h, then cooled to room temperature. After dilution with water, a yellow precipitate was obtained. The crude product was washed with water and acetone. Yield: 81%. ^{1}H NMR (300 MHz, DMSO-d_6, δ): 9.01 (d, acetone). Yield: 81%. ^{1}H NMR (300 MHz, DMSO-d_6, δ): 9.01 (d, J=6.01 Hz, 4H), 8.91 (d, J=6.81 Hz, 4H), 8.17 (s, 2H), 7.81 (d, J=3.81 Hz, 4H), 4.30 (t, 4H), 1.91 (4H), 1.51 (d, 4H), 1.25 (m, 8H), 1.01 (m, 16H), 0.52 (m, 3H). ^{13}C NMR (75 MHz, DMSO-d_6) δ 152.91, 150.02, 146.32, 144.61, 136.44, 126.89, 123.51, 117.56, 112.53, 69.23, 31.91, 29.71, 29.41, 26.01, 22.81, 14.12. Mass spectrometry (MS): m/z 771.06 ([M]$^+$), found m/z 772.0. Element Anal. Calcd for $C_{44}H_{42}N_8O_2$: C, 68.63 H, 6.92 N, 13.67. Found: C, 68.55 H, 6.68 N, 13.52.

*4.3.2. 2-(4-(1H-Imidazo[4,5-f][1,10]phenanthrolin-2-yl))-3,5-(dihexyldithieno[3,2-b:2′3′-d]thioeno)-1H-imidazo[4,5-f][1,10]phenanthroline (**L2**).* A mixture of 1,10-phenanthroline-5,6-dione (215.3 mg, 1.0 mmol), 3,5-dihexyldithieno[3,2-*b*:2′3′-*d*]thiophene-2,6-dialdehyde (223.2 mg, 1.0 mmol), ammonium acetate (1568.9 mg, 20.4 mmol), and glacial acetic acid (30 ml) was refluxed for 2 h. The reaction procedure was the same as that of **L1**. The crude product was washed with water and acetone. Yield: 65%. ^{1}H NMR (300 MHz, DMSO-d_6), δ 9.01 (d, 4H), 8.91 (d, 4H), 7.81 (d, 4H), 2.5 (4H), 1.89 (4H), 1.32 (16H), 0.96 (m, 6H). ^{13}C NMR (75 MHz, DMSO-d_6) δ 154.11, 150.01, 148.01, 141.52, 138.32, 136.44, 135.21, 133.62, 130.21, 129.01, 12,801, 127.49, 126.32, 125.78, 12,421, 122.91, 121.51, 31.91, 29.01, 22.81, 21.31, 14.11. Mass spectrometry (MS): m/z 801.7 ([M]$^+$), found m/z 801.3. Element Anal. Calcd for $C_{46}H_{40}N_8S_3$: C, 68.97 H, 5.03 N, 13.99. Found: C, 68.82 H, 5.19 N, 14.02.

4.4. General synthetic procedure for metallo-polymers P1–P4

The synthetic routes and chemical structures of metallo-polymers are shown in Scheme 1 and Fig. 1, respectively. All of the polymerization procedures were carried out through the metal–ligand coordination reactions.

4.4.1. P1. To a solution of ligand **L1** (1 mmol) in 10 ml of DMF, Rubpy (1 mmol) in DMF (10 ml) was added. The resulting solution was heated to react at 100 °C under a nitrogen atmosphere. After stirring for 24 h, excess NH_4PF_6 was added into the hot solution. The resulting solution was poured into water and the precipitate obtained was purified by repeated precipitations using acetone and water. The polymer was dried under vacuum at 60 °C for 24 h and collected as black solids. Yield: 85%. ^{1}H NMR spectrum of metallo-polymer (**P1**) is similar to that of ligand (**L1**) but broader than peak of ligand. (see Fig. 2) The phenomenon reveals a metallo-polymer (**P1**) was made. ^{1}H NMR (300 MHz, DMSO-d_6, δ): 9.01 (br, 4H), 8.91 (br, 4H), 8.17 (br, 2H), 7.81 (br, 4H), 4.30 (br, 4H), 1.91 (br, 4H), 1.51 (br, 4H), 1.25 (br, 8H), 1.01 (br, 16H), 0.52 (br, 3H).

4.4.2. P2. To a solution of ligand (**L2**) (1 mmol) in 10 ml of DMF, Rubpy (1 mmol) in DMF (10 ml) was added. The resulting solution was heated to react at 100 °C under nitrogen. After stirring for 24 h,

excess NH_4PF_6 was added into the hot solution. The resulting solution was poured into water and the precipitate obtained was purified by repeated precipitations using acetone and water. The polymer was dried under vacuum at 60 °C for 24 h and collected as black solids. Yield: 65%. ^{1}H NMR spectrum of metallo-polymer (**P2**) is similar to that of ligand (**L2**), but **P2** has broader peaks than ligand **L2** (see Fig. 3), which reveals the formation of metallo-polymer **P2**. ^{1}H NMR (300 MHz, DMSO-d_6, δ): 9.01 (br, 4H), 8.91 (br, 4H), 7.81 (br, 4H).

4.4.3. P3. The procedure is analogous to that described for **P1**. Yield: 70%. ^{1}H NMR spectrum of metallo-polymer (**P3**) is similar to that of ligand (**L1**), but **P3** has broader peaks than ligand **L1** (see Fig. 2), which reveals the formation of metallo-polymer **P3** with worse solubility due to the carboxylic acid pendants. ^{1}H NMR (300 MHz, DMSO-d_6, δ): 9.01 (br, 4H), 8.91 (br, 4H), 8.17 (br, 2H), 7.81 (br, 4H), 4.30 (br, 4H).

4.4.4. P4. The procedure is analogous to that described for **P2**. Yield: 54%. ^{1}H NMR spectrum of metallo-polymer (**P4**) is similar to that of ligand (**L2**), but **P4** has broader peaks than ligand **L2** (see Fig. 3), which reveals the formation of metallo-polymer **P4** with worse solubility due to the carboxylic acid pendants. ^{1}H NMR (300 MHz, DMSO-d_6, δ): 9.01 (br, 4H), 8.91 (br, 4H), 7.81 (br, 4H).

4.5. Preparation of nanocomposites complexes

As shown in Fig. 6, all nanocomposites **P1**/**ZnOpy**, **P2**/**ZnOpy**, **P3**/**ZnOpy**, and **P4**/**ZnOpy** were prepared by blending 1 mol **ZnOpy** nanoparticles (**ZnOpy** as proton acceptor) with 1 mol repeating units of metallo-polymers (**P1**–**P4** as proton donors) in the solutions of *N*,*N*-dimethylformamide (DMF), which were self-assembled into supramolecules by evaporating solvents slowly. For example, metallo-polymer **P1** and pyridyl H-acceptor (**ZnOpy**) were dissolved in a DMF solvent and self-assembled into supramolecules by evaporating solvents slowly. When the solvent was evaporated completely, a brown nanocomposites of **P1**/**ZnOpy** was formed. A series of nanocomposites **P1**/**ZnOpy**, **P2**/**ZnOpy**, **P3**/**ZnOpy**, and **P4**/**ZnOpy** were also provided. All anhydrous reactions were carried out avoiding moisture by standard procedures under nitrogen atmosphere.

Acknowledgements

We are grateful to the National Center for High-performance Computing for computer time and facilities. The powder XRD measurements are supported by beamline BL13A (charged by Dr. Ming-Tao Lee) of the National Synchrotron Radiation Research Center (NSRRC) in Taiwan. The financial supports of this project provided by the National Science Council of Taiwan (ROC) through NSC 99-2113-M-009-006-MY2 and NSC 99-2221-E-009-008-MY2 are acknowledged.

References and notes

1. (a) Gong, D. R.; Wang, B. L.; Bai, C. X.; Bi, J. F.; Wang, F.; Dong, W. M.; Zhang, X. Q.; Jiang, L. S. *Polymer* **2009**, *50*, 6259–6264; (b) Zhao, X.; Luo, X. X.; Li, B.; Song, H. B.; Xu, S. S.; Wang, B. Q. *Eur. Polym. J.* **2008**, *44*, 3264–3270.
2. (a) Zhu, X. J.; Holliday, B. J. *Macromol. Rapid Commun.* **2010**, *3*, 904–909; (b) Guchhait, A.; Rath, A. K.; Pal, A. J. *Chem. Mater.* **2009**, *21*, 5292–5299; (c) Skompska, M. *Synth. Met.* **2010**, *160*, 1–15.
3. (a) Chan, H. T.; Mak, C. S. K.; Djurisic, A. B.; Chan, W. K. *Macromol. Chem. Phys.* **2011**, *212*, 774–784; (b) Cheung, W. K.; Mak, C. S. K.; Chan, W. K. *Macromol. Rapid Commun.* **2012**, *33*, 585–591.
4. (a) Burnworth, M.; Mendez, J. D.; Schroeter, M.; Rowan, S. J.; Weder, C. *Macromolecules* **2008**, *41*, 2157–2163; (b) Pefkianakis, E. K.; Tzanetos, N. P.; Kallitsis, J. K. *Chem. Mater.* **2008**, *20*, 6254–6262; (c) Happ, B.; Friebe, C.; Winter, A.; Hager, M. D.; Schubert, U. S. *Eur. Polym. J.* **2009**, *45*, 3433–3441; (d) Sun, T. X.; Wang, Q.; Fan, Z. Q. *Polymer* **2010**, *51*, 3091–3098.
5. (a) Dong, T. Y.; Lin, M. C.; Chang, S. W.; Ho, C. C.; Lin, S. F.; Lee, L. *J. Org. Chem.* **2007**, *692*, 2324–2333; (b) Winter, A.; Friebe, C.; Chiper, M.; Hager, M. D.; Schubert, U. S. *J. Polym. Sci., Part A: Polym. Chem.* **2009**, *47*, 4083–4098.
6. (a) Schulz, G. L.; Holdcroft, S. *Chem. Mater.* **2008**, *20*, 5351–5355; (b) Williams, K. A.; Boydston, A. J.; Bielawski, C. W. *Chem. Soc. Rev.* **2007**, *36*, 729–744; (c) Yıldırım, M. M.; Kaya, I. M. *Polymer* **2009**, *50*, 5653–5660.
7. (a) Schlutter, F.; Wild, A.; Winter, A.; Hager, M. D.; Baumgaertel, A.; Friebe, C.; Schubert, U. S. *Macromolecules* **2010**, *43*, 2759–2771; (b) Qi, S. L.; Wu, Z. P.; Wu, D. H.; Yang, W. T.; Jin, R. G. *Polymer* **2009**, *50*, 845–854.
8. (a) Padhy, H.; Sahu, D.; Chiang, I. H.; Patra, D.; Kekuda, D.; Chu, C. W.; Lin, H. C. *J. Mater. Chem.* **2011**, *21*, 1196–1205; (b) Ramiro, P.; García-Fresnadillo, D.; Orellana, G. *Tetrahedron* **2005**, *61*, 9478–9483; (c) Lee, C. H.; Zhang, Y. Y.; Romayanantakit, A.; Galoppini, E. *Tetrahedron* **2010**, *66*, 3897–3903.
9. Yao, C. J.; Zhong, Y. W.; Nie, H. J.; Abruna, H. D.; Yao, J. *J. Am. Chem. Soc.* **2011**, *133*, 20720–20723.
10. (a) Milum, K. M.; Kim, Y. N.; Holliday, B. J. *Chem. Mater.* **2010**, *22*, 2414–2416; (b) Zhuang, J. P.; Zhou, W. D.; Li, X. F.; Li, Y. J.; Wang, N.; He, X. R.; Liu, H. B.; Li, Y. L.; Jiang, L.; Huang, C. S.; Cui, S.; Wang, S.; Zhu, D. B. *Tetrahedron* **2005**, *61*, 8686–8693; (c) Eda, Y.; Itoh, K.; Ito, Y. N.; Kawato, T. *Tetrahedron* **2009**, *65*, 282–288.
11. (a) Wild, A.; Schlutter, F.; Pavlov, G. M.; Friebe, C.; Festag, G.; Winter, A.; Hager, M. D.; Cimrova', V.; Schubert, U. S. *Macromol. Rapid Commun.* **2010**, *31*, 868–874; (b) Banjoko, V.; Xu, Y. Q.; Mintz, E.; Pang, Y. *Polymer* **2009**, *50*, 2001–2009.
12. Wild, A.; Friebe, C.; Winter, A.; Hager, M. D.; Grummt, U. W.; Schubert, U. S. *Eur. J. Org. Chem.* **2010**, *10*, 1859–1868.
13. (a) Constable, E. C. *Chem. Soc. Rev.* **2007**, *36*, 246–253; (b) Kim, B. S.; Basavaraja, C.; Jo, E. A.; Kim, D. G.; Huh, D. S. *Polymer* **2010**, *51*, 3365–3371.
14. (a) Miyashita, N.; Kurth, D. G. *J. Mater. Chem.* **2008**, *23*, 2636–2649; (b) Batista, R. M. F.; Costa, S. P. G.; Belsley, M.; Lodeiro, C.; Raposo, M. M. M. *Tetrahedron* **2008**, *64*, 9230–9238.
15. (a) He, M.; Zhang, F. *J. Org. Chem.* **2007**, *72*, 442–451; (b) Fang, H. P.; Lin, J. W.; Chiang, I. H.; Chu, C. W.; Wei, K. H.; Lin, H. C. *J. Polym. Sci. Part A: Polym. Chem.*, in press.
16. (a) Chan, W. K. *Coord. Chem. Rev.* **2007**, *251*, 2104–2118; (b) Torres, T.; Gouloumis, A.; Garcia, D. S.; Jayawickramarajah, J.; Seitz, W.; Guldi, D. M.; Sessler, J. L. *Chem. Commun.* **2007**, 292–294; (c) Chen, B. K.; Zhong, H. Z.; Li, R.; Zhou, Y.; Ding, Y. Q.; Li, Y. F.; Zou, B. S. *Sci. Adv. Mater.* **2012**, *4*, 342–345.
17. Wessendorf, F.; Gnichwitz, J. F.; Sarova, G. H.; Hager, K.; Hartnagel, U.; Guldi, D. M.; Hirsch, A. *J. Am. Chem. Soc.* **2007**, *129*, 16057–16071.
18. (a) Koster, L. J. A.; Strien, W. J. V.; Beek, W. J. E.; Blom, P. W. M. *Adv. Funct. Mater.* **2007**, *17*, 1297–1302; (b) Chu, C. C.; Raffy, G.; Ray, D.; Guerzo, A. D.; Kauffmann, B.; Wantz, G.; Hirsch, L.; Bassani, D. M. *J. Am. Chem. Soc.* **2010**, *132*, 12717–12723.
19. Sahu, D.; Padhy, H.; Patra, D.; Yin, J. F.; Hsu, Y. C.; Lin, J. T.; Lu, K. L.; Wei, K. H.; Lin, H. C. *Tetrahedron* **2011**, *67*, 303–311.
20. (a) Fang, H. P.; Chiang, I. H.; Chu, C. W.; Yang, C. C.; Lin, H. C. *Thin Solid Films* **2011**, *519*, 5212–5218; (b) Jiu, T. G.; Liu, H. B.; Fu, L. M.; He, X. R.; Wang, N.; Li, Y. L.; Ai, X. C.; Zhu, D. B. *Chem. Phys. Lett.* **2004**, *398*, 113–117; (c) Liu, H. B.; Zuo, Z. C.; Guo, Y. B.; Li, Y. J.; Li, Y. L. *Angew. Chem., Int. Ed.* **2010**, *49*, 2705–2707.
21. (a) Puodziukynaite, E.; Oberst, J. L.; Dyer, A. L.; Reynolds, J. R. *J. Am. Chem. Soc.* **2012**, *134*, 968–978.
22. (a) Wang, L. Y.; Tsai, H. Y.; Lin, H. C. *Macromolecules* **2010**, *43*, 1277–1288; (b) Cheng, K. W.; Mak, C. S. C.; Chan, W. K.; Ng, A. M. C.; Djurisic, A. B. *J. Polym. Sci., Part A: Polym. Chem.* **2008**, *46*, 1305–1317.
23. Herrikhuyzen, V.; Herrikhuyzen, J. V.; George, S. J.; Vos, M. R. J.; Sommerdijk, A. J. M.; Ajayaghosh, A.; Meskers, S. C. J.; Schenning, A. P. H. J. *Angew. Chem., Int. Ed.* **2007**, *19*, 1825–1828.
24. Xu, J.; Wang, J.; Mitchell, M.; Mukherjee, P.; Jeffries-EL, M.; Petrich, J. W.; Lin, Z. *J. Am. Chem. Soc.* **2007**, *129*, 12828–12833.
25. Motaung, D. E.; Malgas, G. F.; Arendse, C. J. *J. Mater. Sci.* **2010**, *45*, 3276–3283.
26. Koppe, M.; Scharber, M.; Brabec, C.; Duffy, W.; Heeney, M.; McCulloch, I. *Adv. Funct. Mater.* **2007**, *17*, 1371–1376.
27. Li, K. C.; Huang, J. H.; Hsu, Y. C.; Huang, P. J.; Chu, C. W.; Lin, J. T.; Ho, K. C.; Wei, K. H.; Lin, H. C. *Macromolecules* **2009**, *42*, 3681–3693.
28. Lim, E.; Lee, S.; Lee, K. K. *Chem. Commun.* **2011**, 914–916.
29. Li, H.; Jiang, P.; Yi, C.; Li, C.; Liu, S. X.; Tan, S. T.; Zhao, B.; Braun, J.; Meier, W.; Wandlowski, T.; Decurtins, S. *Macromolecules* **2010**, *43*, 8058–8062.
30. Zhang, M.; Fan, H.; Guo, X.; He, Y.; Zhang, Z.; Min, J.; Zhang, J.; Zhao, G.; Zhan, X. W.; Li, Y. F. *Macromolecules* **2010**, *43*, 5706–5712.
31. Zou, Y.; Najari, A.; Berrouard, P.; Beaupre, S.; Aı'ch, B. R.; Tao, Y.; Leclerc, M. *J. Am. Chem. Soc.* **2010**, *132*, 5330–5331.
32. Li, Y. F.; Zou, Y. P. *Adv. Mater.* **2008**, *20*, 2952–2958.
33. Pokrop, R.; Pamuła, K.; Drogomirecka, S. D.; Zagorska, M.; Borysiuk, J.; Reiss, P.; Pron, A. *J. Phys. Chem. C* **2009**, *113*, 3487–3493.
34. Lai, C. H.; Lee, W. F.; Wu, I. C.; Kang, C. C.; Chen, D. Y.; Chen, L. J.; Chou, P. T. *J. Mater. Chem.* **2009**, *19*, 7284–7289.